www.adpr-journal.com

In-Plane and Out-of-Plane Optical Properties of Monolayer, Few-Layer, and Thin-Film MoS₂ from 190 to 1700 nm and Their Application in Photonic Device Design

Kazi M. Islam,* Ron Synowicki, Timothy Ismael, Isaac Oguntoye, Nathan Grinalds, and Matthew D. Escarra

Monolayer, few-layer, and thin-film MoS2 is synthesized using chemical vapor deposition (CVD) and thermal vapor sulfurization (TVS) methods. The complex refractive index of these samples is assessed using variable angle spectroscopic ellipsometry (VASE) measurements over a broad spectral range between 190 and 1700 nm. The ellipsometry data are sensitive to birefringence effects in the thickest thin-film sample. These birefringence effects are investigated, and an analysis method is developed to extract the in-plane and out-of-plane optical properties. The complex refractive index is then used to calculate reflectance, transmittance, and absorption of the MoS2 films using the transfer-matrix method (TMM) and is matched with experimentally measured transmittance of the same samples. The modeled results show that the monolayer, few-layer, and thin-film MoS₂ absorbs 7.4%, 12.6%, and 32.4% of the incident light, respectively, between 300 and 700 nm. When normalized to per unit-thickness absorption, they absorb 12.1%, 5.9%, and 1.1% nm⁻¹, respectively, clearly showing superior light-matter interaction in the monolayer and few-layer films. These new complex refractive index data are further used to design optical coatings for these films to either confine absorption in a narrow bandwidth for photodetector applications or enhance broadband absorption for photovoltaic applications.

1. Introduction

The 2D materials have gained much interest in the last decade due to their unique electrical, optical, and mechanical properties

Dr. K. M. Islam, T. Ismael, I. Oguntoye, N. Grinalds, Dr. M. D. Escarra Department of Physics & Engineering Physics Tulane University

New Orleans, LA 70118, USA E-mail: kislam@tulane.edu

R. Synowicki Measurements Lab J. A. Woollam Co., Inc. Lincoln, NE 68508, USA

The ORCID identification number(s) for the author(s) of this article can be found under https://doi.org/10.1002/adpr.202000180.

© 2021 The Authors. Advanced Photonics Research published by Wiley-VCH GmbH. This is an open access article under the terms of the Creative Commons Attribution License, which permits use, distribution and reproduction in any medium, provided the original work is properly cited.

DOI: 10.1002/adpr.202000180

exhibited in their atomically thin layers that are, otherwise, not present in their bulk counterparts.^[1] Among the 2D materials, one distinct family of materials known as transition metal dichalcogenides (TMDCs) exhibits very promising electronic and optical properties for applications in optoelectronics due to their strong light-matter interactions.^[2] TMDCs generally have the chemical structure of MX2, where "M" is either Mo or W, and "X" is S, Se, or Te. In particular, molybdenum disulfide (MoS₂) is one of the most studied materials in the past several years due to its relatively high carrier mobility and strong photoluminescence (PL) properties as a semiconducting material, making it a compelling candidate for 2D material-based optoelectronics, such as photodetectors, transistors, and photovoltaics. [3] MoS₂ has a large direct optical bandgap of 1.85 eV in the monolayer compared with its 1.3 eV indirect bandgap in the bulk^[4,5] and has a high carrier mobility of 200 cm² V⁻¹ s⁻¹ and an on-off ratio of 108 for field-effect

transistors. ^[6] However, most studies on these materials have been done on exfoliated layers that are limited by lateral dimension and are not scalable. After the initial proof-of-concept stage, research is now moving toward synthesized 2D MoS_2 that is scalable, with precise thickness control and uniform coverage. The properties of 2D layers are not always consistent between exfoliated single crystal materials and large-area synthesized films, which calls for further study on these synthesized materials. ^[7]

Several synthesis methods have been reported, including chemical vapor deposition (CVD) of monolayer MoS_2 using MoO_3 and S precursors. [8,9] While this method produces uniform and high-quality monolayer and bilayer films, precise thickness control for few layers or even thin films of MoS_2 is challenging with this. On the other hand, thermal vapor sulfurization (TVS) that utilizes sulfurization of a precursor Mo film on the substrate has great control over thickness. In this method, the final MoS_2 film thickness directly depends on the precursor Mo film thickness. [10] To its disadvantage, this method is not preferred to grow monolayer films, as it suffers from nonuniformity in lateral and vertical growth, resulting in

www.advancedsciencenews.com

www.adpr-journal.com

4DVANCED

including the phase difference between the p- and s-polarized components.^[23–25] For example, ellipsometry is commonly used to determine the thickness of native oxide films on semiconductor wafers and is effective for extremely thin films down to the monolayer level, such as those studied in this work.

The monolayer sample studied here was grown by the CVD method, whereas the few-layer and thin-film samples were grown by the TVS method. The films were also characterized by Raman spectroscopy, PL, atomic force microscopy (AFM), and UV–Vis–near-IR (NIR) spectroscopy for quality and thickness validation. The complex refractive index was used to model reflectance, transmittance, and absorption using the transfermatrix method (TMM) and matched with experimentally measured data. Finally, an optical model was built to study the effect of utilizing various optical coatings to confine absorption in a narrow bandwidth or to enhance broadband absorption in monolayer, few-layer, and thin-film MoS₂ for various optoelectronic applications, such as photodetectors, sensors, and photovoltaics.

inhomogeneous submonolayer growth, small grain sizes, and poor transport properties, i.e., low electron/hole mobility.

Despite the advances in these and other growth methods, the fundamental electronic and optical properties of these films still require better understanding. As these 2D materials have been proposed and demonstrated to have superior characteristics in optoelectronic device applications, such as transistors, photoelectrons, photoemitters, and photovoltaics, understanding how these materials interact with different bandwidths of light at various thicknesses is crucial. While monolayer films exhibit the maximum PL, they only absorb on the order of 10% of the visible spectrum. [11] Hence, a few-layer film or even a thicker thin film ($\approx > 3$ nm thick that shows bulk-like properties [12]) of MoS₂ is possibly a better candidate for some optoelectronic applications, e.g., photovoltaics.

The complex refractive index is the most fundamental material property that describes the light-matter interaction in these 2D MoS₂ layers. Several previous reports have shed light on the complex refractive index (or the complex dielectric function, where one can be calculated from the other) of monolayer and few-layer MoS₂.^[13-17] Many of these reports have been indirect calculations of the n and k values, whereas some direct measurements are performed only for a small bandwidth of the spectrum. Li et al. reported the complex dielectric function of exfoliated monolayer TMDC materials, including MoS2, from reflection spectra using Kramers-Kronig analysis. [11] As reflection spectroscopy depends on light intensity, and thus all reflected light needs to be collected from the samples, these measurements are difficult to do accurately. Also, intensity-based techniques are generally dependent on interference effects, which are not present for very thin films and are, thus, less sensitive to low-dimensional materials with small thicknesses. Shen et al. and Liu et al. reported the complex refractive index of 2D MoS₂ using spectroscopic ellipsometry for only monolayer materials. [13,18] On the other hand, Yim et al. reported n and kdata for few-layer MoS2 samples grown by the TVS method between 380 and 900 nm using ellipsometry at a single angle of incidence. [19] Li et al. and Park et al. also reported the complex refractive index of few-layer MoS2 films grown by TVS and CVD methods, respectively, using a spectroscopic ellipsometry up to 1240 nm. [20,21] Finally, a recent report by Ermolaev et al. shows the complex refractive index of monolayer and bulk MoS2 in the 290-3300 nm spectral range but does not include interesting data in the UV region below $290 \text{ nm.}^{[22]}$

In this work, we report variable angle spectroscopic ellipsometry (VASE) measurement and subsequent extraction of the complex refractive index of monolayer, few-layer, and thicker thin-film MoS_2 . The reported data range from 190 to 1700 nm, covering a wide range of incident angles and wavelengths. Acquisition of spectroscopic data allows the determination of the optical properties (n and k) in transparent and absorbing regions over the widest possible spectral range. Data acquisition at multiple angles is desirable, as each angle presents a different path length through the film stack, and all angles can be analyzed simultaneously for film thicknesses.

VASE is a nondestructive characterization method that has great potential for studying 2D films because of its higher sensitivity to small thickness changes, resulting primarily from the measurement of the polarization state instead of intensity,

2. Sample Preparation

Monolayer MoS2 films were grown using the CVD method, as it provides good film quality in this thickness regime, whereas the TVS method was used to grow few-layer and thin-film MoS₂ for its better thickness control. Figure 1 shows a schematic of the three-zone furnace used for both the CVD and TVS growth. For the monolayer films, MoO₃ and S powders were placed inside a 1 in. tube. The tube is initially pumped down to 15 mTorr base pressure, and then, Ar is flowed as a carrier gas at 2.5 sccm flow rate. Sapphire substrates were placed growth-face-down on a ceramic crucible that contains the MoO₃ powder and is set in the second zone of the furnace at 750 °C, as shown in Figure 1 (top). Sulfur powder is kept in a crucible in the first zone at 120 °C. The spacing between two crucibles is optimized to be around 30 cm. The ramp time to 750 °C is 30 min, and the deposition is carried on for 10 min. The tube pressure is maintained at 2.4 Torr during deposition. After the deposition, the monolayer MoS2 films are transferred to a SiO2-on-Si substrate for characterization. [26] For the TVS method, a Mo precursor film was grown on sapphire or SiO2-on-Si substrates using electron-beam evaporation, where the thickness of the precursor Mo film determines the final MoS₂ thickness.^[10] The substrate is then placed in the third zone for growth on the top side, and S powder is loaded on a crucible in the first zone of the furnace, as shown in Figure 1 (bottom). The spacing between the two crucibles in this case is optimized to be around 50 cm. The tube is then pumped down to a 15 mTorr base pressure, and Ar carrier gas flows at 100 sccm flow rate. The temperature in the third zone is set at 900 °C with a 90 min ramp time, and the first zone is set at 120 °C. The deposition is carried out for 10 min while the pressure in the tube is maintained at 1.2 Torr. The evolution from Mo to MoS2 is characterized in steps, as shown in Section S1, Supporting Information.

3. Optical Property Characterization

The samples were characterized for quality and precise thickness control using Raman spectroscopy, PL, AFM, VASE, and



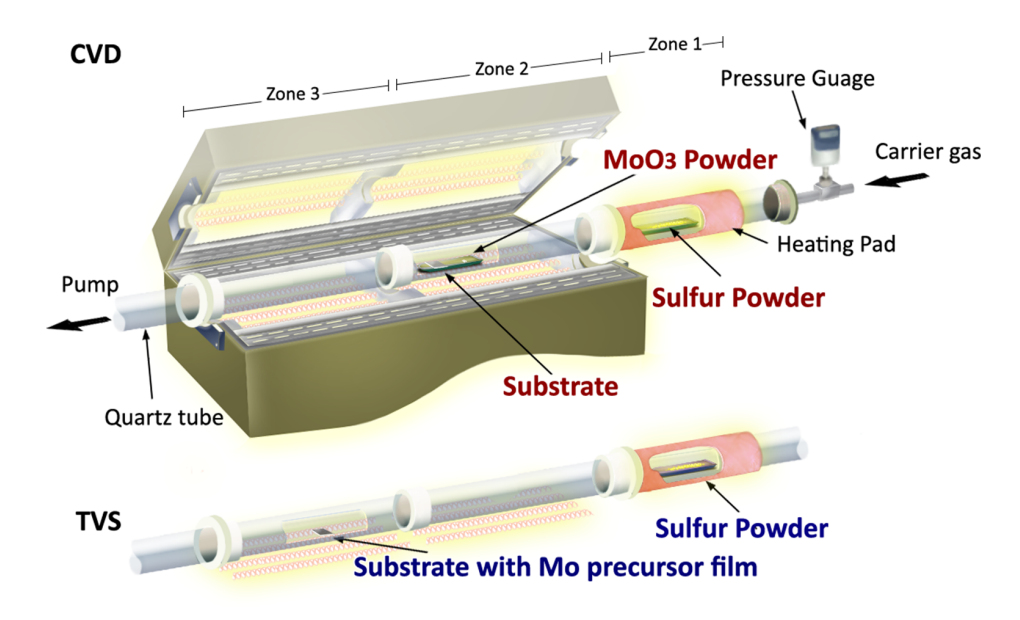


Figure 1. Schematic of the two synthesis methods used in this study: CVD and thermal vapor transport (TVS). A standard two-zone furnace is modified to have a third zone for low-temperature sulfur (S) evaporation and to increase the distance between the S source and the growth substrate.

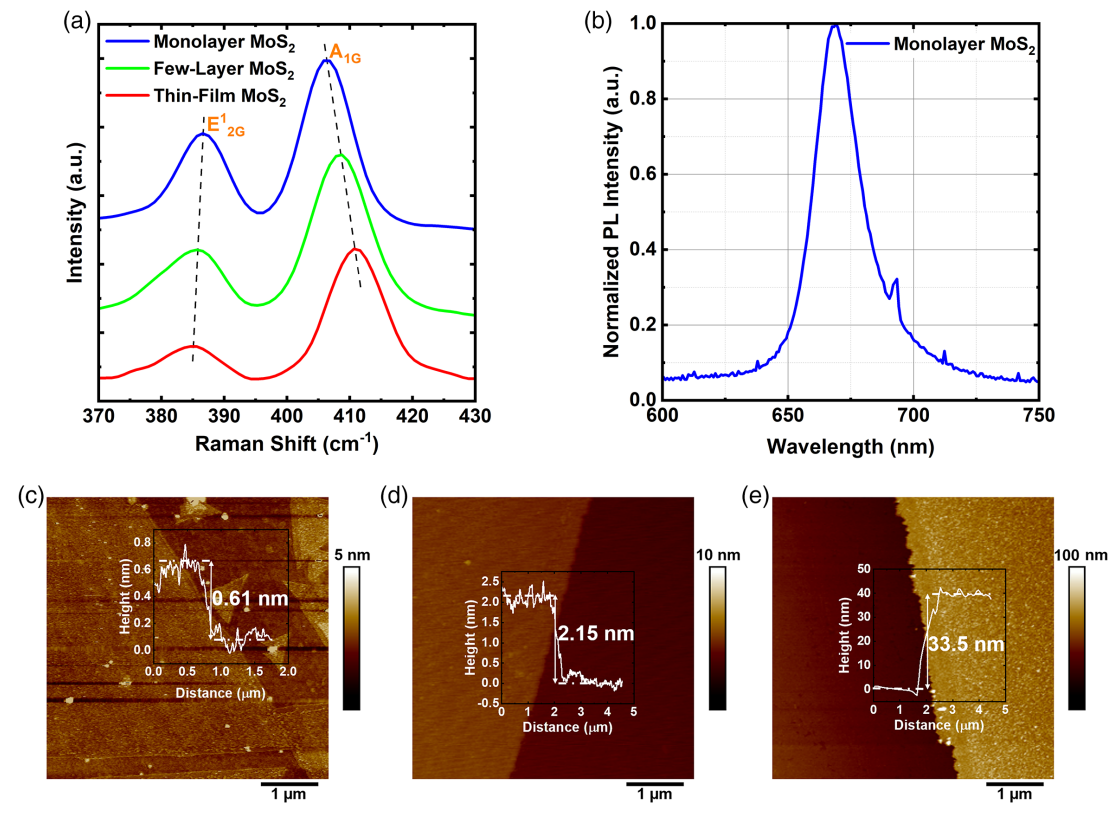


Figure 2. a) Raman characterization of the CVD and TVS grown MoS_2 samples on SiO_2 -on-Si substrates using a 532 nm laser source. b) PL spectra of a monolayer MoS_2 sample with an emission peak near 670 nm, using a 405 nm excitation source. AFM images showing step height and topography of the c) monolayer, d) few-layer, and e) thin-film MoS_2 samples.

UV–Vis–NIR spectroscopy. **Figure 2**a shows the Raman scattering plots of monolayer, few-layer, and thin-film MoS₂ samples. The E^1_{2G} and A_{1G} peaks are located at 386.5 and 406 cm⁻¹,

respectively, for monolayer MoS_2 , at 386 and 408.5 cm $^{-1}$, respectively, for few-layer MoS_2 , and at 385.5 and 411 cm $^{-1}$, respectively, for thin-film MoS_2 . The 19.5, 22.5, and 25.5 cm $^{-1}$



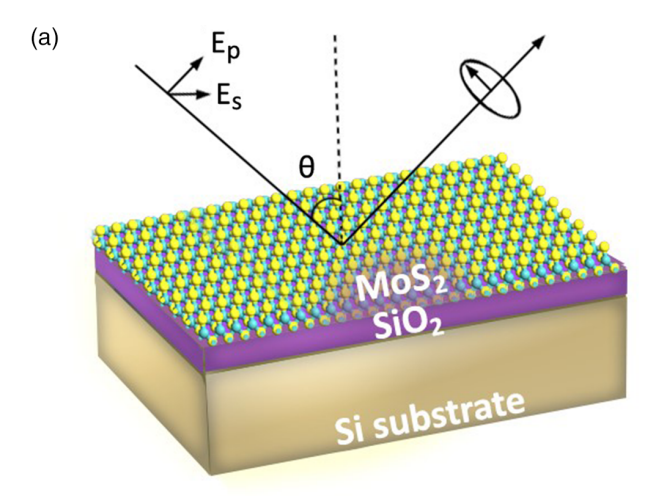
spacings between the $E^1_{2\rm G}$ and $A_{1\rm G}$ peaks are consistent with previous reports, [12] confirming their respective thicknesses. Figure 2b shows the normalized PL intensity of as-grown monolayer ${\rm MoS_2}$ on a sapphire substrate, showing the excitonic A-peak at \approx 670 nm. The excitonic peak blue shifts for ${\rm MoS_2}$ samples transferred onto ${\rm SiO_2}$ -on-Si samples, as shown in Figure S1, Supporting Information, due to substrate-induced strain and relaxation. [27,28] The PL peak has 20.2 nm full width at half maximum (FWHM), confirming good optical quality. This PL is a signature characteristic of monolayer TMDC films.

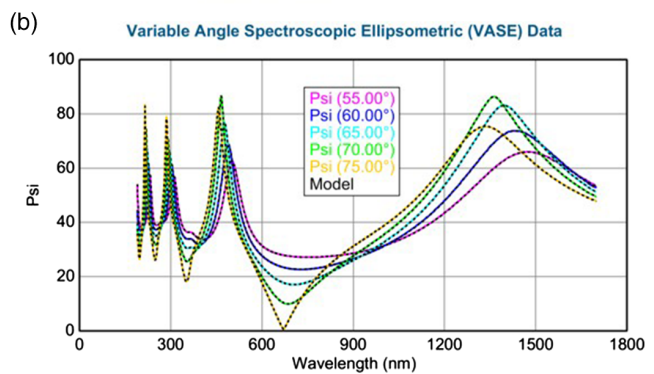
Figure 2c–e shows the AFM topography of the three samples. The average step height is measured as 0.61, 2.15, and 33.5 nm for the "monolayer," "few-layer," and "thin-film" samples, respectively. The samples were measured for step heights at three different locations within a cm² area, and the film thickness variation is within $\pm 10\%$, showing good uniformity. The UV–Vis–NIR spectroscopy was also used to measure transmittance across a cm-scale sample to confirm uniformity of optical properties, as shown in Figure S4, Supporting Information.

Ellipsometry measures the change in polarization state of light reflected from or transmitted through a sample. The principle of reflection-mode ellipsometry is shown in **Figure 3**a where the change in polarization caused by the sample is recorded as two experimentally measured values Ψ and Δ . This process is repeated for a plurality of angles and wavelengths using the VASE technique. Data were acquired at five angles of incidence from 55° to 75° in steps of 5° and over the spectral range from 190 to 1700 nm. All angles and wavelengths were fit simultaneously in the data analysis. Figure 3b,c shows the experimentally measured Ψ and Δ data as solid curves along with the model fitted data as dotted curves generated by the data analysis for the monolayer MoS₂ film.

To extract properties of interest about a sample, such as film thickness and optical constants n and k, ellipsometry data analysis requires constructing an optical model to match the experimentally measured Ψ and Δ values. The optical model contains the optical constants n and k of the substrate, as well as the thickness and optical constants *n* and *k* of each layer in the stack. The data analysis software allows for fixing some properties of the model while allowing some parameters to be defined as adjustable variables. The analysis software adjusts the variable parameters to find the best match to fit the experimental Ψ and Δ curves by minimizing a goodness of fit parameter defined as the mean squared error (MSE). [23-25] In this work, the optical constants of the silicon substrate, thermal SiO₂ layer, and 1 nm interface layer were taken from published values and not allowed to vary^[29] and are not expected to change noticeably after film deposition and thermal processing. This was confirmed by measuring an identical substrate of thermal SiO2 on Si before and after thermal processing but with no film deposition. The goodness of fit, SiO2 thickness, and optical model were identical before and after heating, as shown in Figure S5, Supporting Information.

Determining the optical constants n and k of thin films via ellipsometry is generally more accurate for thicker films due to longer path length in the film. In this work, we first analyzed the thickest "thin-film" MoS_2 for film thickness and optical constants, and then attempted to apply these optical constants to the very thin monolayer and few-layer MoS_2 films by keeping the





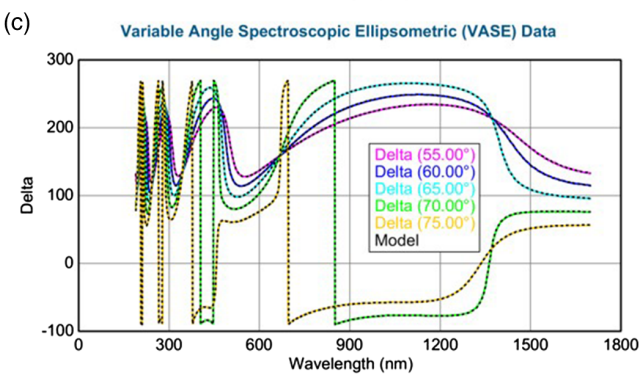


Figure 3. a) Schematic of the spectroscopic ellipsometry measurements showing the optical model of the MoS_2 – SiO_2 –Si samples. Measured and modeled b) Ψ and c) Δ spectra of monolayer MoS_2 versus wavelength. The solid colored lines are measured data at various angles of incidence, and the dashed black lines are modeled fit values with good agreement obtained over the full spectral range.

optical constants fixed from the thicker film and fitting only the film thickness. It was found that the monolayer and few-layer samples did not analyze well using optical constants from the thickest sample, demonstrating the sensitivity of the optical constants to film thickness.

A further complication is the few-layer and thin-film MoS_2 films tended to show some level of nonzero absorption over the entire measured spectral range. To maximize sensitivity to the optical constants of such thin absorbing films, we applied the

ADVANCED PHOTONICS RESEARCH

techniques of multiple angles of incidence, optical constant parameterization, and interference enhancement discussed by McGahan et al. [30,31] and Hilfiker et al. [32] For interference enhancement, the thin absorbing film is deposited over a much thicker transparent film, such as 300 nm thermal SiO₂ in this work. This places the thin absorbing MoS₂ film between the transparent ambient above and the transparent SiO₂ film underneath, which allows absorption in the MoS₂ film to affect the amplitude of interference features in the Ψ and Δ spectra caused by the thick transparent SiO₂ film underneath.

As the MoS_2 films are so thin, parameterizing the optical constants via a dispersion model for the optical constants works well, particularly when the model enforces Kramers–Kronig consistency on the shape of the n and k curves. A dispersion model also allows the data to be fit using a minimum number of adjustable parameters.

Earlier published works investigated combinations of Lorentz, $^{[13,18,20,21]}$ single Tauc–Lorentz, $^{[19]}$ and multiple Tauc–Lorentz dispersion models with separate bandgaps for each Tauc–Lorentz term. $^{[22]}$ In addition, all the models to analyze MoS $_2$ in these previous works were isotropic and did not investigate birefringence in the MoS $_2$.

In this work, a variety of dispersion models enforcing Kramers-Kronig consistency were investigated, including Lorentz, Tauc-Lorentz, Sellmeier, Gaussian, and combinations of these. [33,34] We also used a Kramers-Kronig consistent B-Spline model for MoS₂ optical constants.^[34] Advantages of the B-Spline model include maximum flexibility to the line shape of the dielectric function, including the exciton peaks of MoS₂, without assuming the fixed line shapes of Lorentz, Gaussian, or other function for each oscillator. The B-Spline node spacing is also adjustable throughout the fitted spectral range, allowing for extra resolution to be defined through regions of interest such as the exciton peaks. Furthermore, the B-Spline analysis of MoS₂ in this work did not require additional parameters such as offsets to the real part of the dielectric function or Sellmeier Pole functions to fit the data, whereas analysis with Gaussian, Lorentz, or Tauc-Lorentz functions did require these extra adjustments. The B-Spline fits also showed a slightly better goodness of fit via a lower MSE value, resulting primarily from the extra flexibility of the B-Spline line shape.

Each sample was fit first to an isotropic model with no birefringence in the MoS₂ index, similar to previous works mentioned. Adding birefringence to allow different optical properties in-plane (ordinary index) and out-of-plane (extraordinary index) improved the fit significantly for the thickest thin-film sample, likely due to the longer path length through this thicker film with more layers in the layered structure. The in-plane optical constants describe the refractive index and absorption features over the full spectral range. In contrast, the out-of-plane refractive index was described using a single Sellmeier dispersion function, similar to the method presented by Hong et al. for analyzing birefringent plastic substrates.^[34] As mentioned by Ermolaev et al., sensitivity to the out-of-plane refractive index is greatly reduced, as light entering the sample propagates near normal to the surface due to the high index of MoS2 and is, thus, much more sensitive to the in-plane index component, justifying use of a simple transparent Sellmeier for the out-of-plane index component.^[22] Thus, the birefringence effect was only seen in

the thickest thin-film MoS₂ sample and only for wavelengths with relatively low absorption. It is likely that the monolayer and few-layer MoS₂ also exhibits anisotropy, though the optical response of the out-of-plane component was not strong enough to definitively conclude that here.

Analysis of each MoS2 film is described as follows.

3.1. Analysis of Thin-Film MoS2

Analysis of the ellipsometric data started with the thickest film, the "thin-film" MoS_2 sample. Isotropic models using B-Spline functions or combinations of Sellmeier and Gaussian functions were fit, followed by testing for birefringence by converting to an anisotropic, birefringent model. The birefringent model showed significant improvement to the psi and delta curves and improved the goodness of fit by over 50%, justifying the addition of uniaxial birefringence to the model. Fitting a surface roughness/oxide layer 8.1 nm thick also significantly improved the fit.

Figure 4 shows the birefringent refractive index *n* and *k* for the thin-film MoS₂ fitted with Gaussian (dotted lines) and B-Spline dispersion functions (solid lines) with nearly identical results. For the Gaussian model, the in-plane refractive index was fitted to 17 Gaussian and one Sellmeier dispersion function with a goodness of fit MSE of 2.089. For the B-Spline fit, the node spacing was set to 0.05 eV over the full range with a goodness of fit MSE of 2.067. For both models, the out-of-plane index was fit to a single transparent Sellmeier model, which assumes no absorption (k=0). Note that in Figure 4, the out-of-plane index (Sellmeier model) is plotted only to 1.3 eV (arbitrarily chosen to match the bandgap of bulk MoS₂), as the material becomes highly absorbing at higher photon energies above the bandgap. As the absorption increases, the sensitivity to the out-of-plane response disappears. The in-plane optical response dominates due to the high index causing the strongly refracted light to propagate almost entirely in-plane in the material. The transverse electric field senses the in-plane optical response much more than the out-of-plane component. Therefore, the ellipsometric

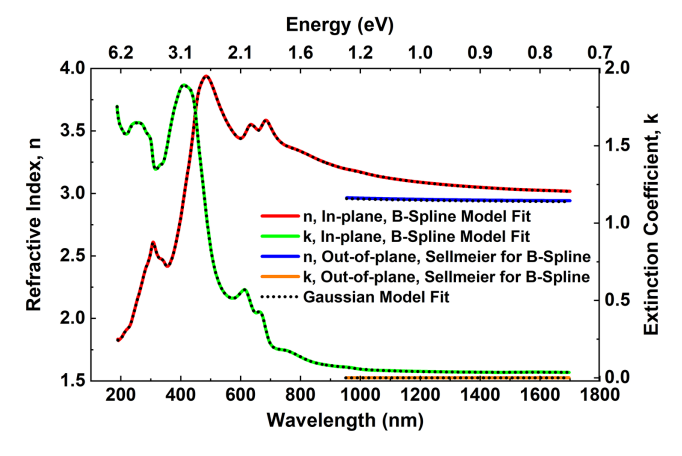


Figure 4. Optical constants n and k for thin-film MoS_2 analyzed using a birefringent model. The in-plane index was fitted using the B-Spline model (solid lines) or a combination of Gaussian and Sellmeier functions (dotted lines) with nearly identical results. The out-of-plane component was fit to a single transparent (k = 0) Sellmeier function plotted above to 1.3 eV.

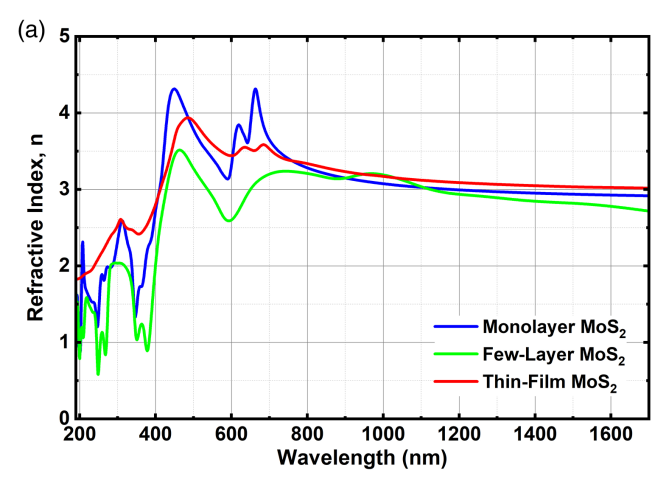
ADVANCED PHOTONICS RESEARCH

www.advancedsciencenews.com www.adpr-journal.com

measurement is sensitive to the in-plane optical response at all wavelengths. However, only in the transparent region below the bandgap, the measurement is sensitive to the birefringence and, thus, sensitive to both the ordinary and extraordinary components of the refractive index.

3.2. Analysis of Few-Layer MoS2

The few-layer MoS_2 sample was also fit to an isotropic model using a Gaussian and Sellmeier dispersion model, where two Sellmeier and six Gaussian functions were used for the Gaussian model fit. The A and B exciton doublet peaks appear blended into a single peak near 1.9 eV. Similar to the thin-film sample, a defect absorption tail is present down to 0.7 eV, as shown in **Figure 5**, again possibly due to incomplete sulfurization of the precursor molybdenum film in the TVS process. The peak near 3 eV is more asymmetric, with a shoulder peak near 3.4 eV. The A and B exciton doublets appear as a single peak in the few-layer film, unlike the monolayer or thin-film sample. This has been observed in the previously published reports. $^{[19]}$



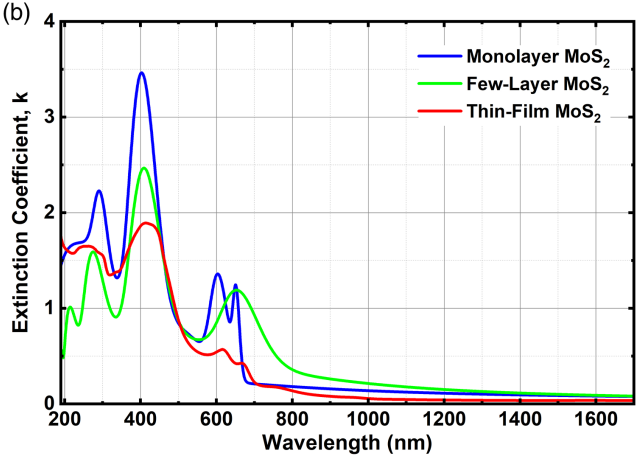


Figure 5. In-plane optical constants, n and k, for monolayer, few-layer, and thin-film MoS_2 . The refractive index, n, is shown at the top, whereas the extinction coefficient, k, is shown at the bottom.

3.3. Analysis of Monolayer MoS₂

The monolayer MoS_2 film was analyzed with an isotropic model using a Gaussian plus Sellmeier model. Two Sellmeier and six Gaussian functions were used for the Gaussian model fit. The positions of the A and B excitons at 1.91 and 2.05 eV, respectively, are blue shifted compared with the thin-film sample analyzed earlier and similar to the values of 1.88 and 2.03 eV reported by Shen et al. [13] The large absorption near 3 eV is prominent, along with additional smaller absorptions that are more prominent than observed in the thin-film sample. The results are consistent with other published data, as shown in Figure S6, Supporting Information.

Figure 5 shows the in-plane refractive index (top) and extinction coefficient (bottom) for all three MoS₂ films plotted above versus wavelength. The thickness of the monolayer, few-layer, and thin-film MoS₂ layers from the ellipsometric measurements was also determined to be in good agreement with the AFMmeasured thicknesses. Adding a surface roughness layer to the thickest film also improved the fits, suggesting that the surface of the thin-film MoS₂ has some roughness and/or surface oxidation. The n and k values are consistent with previously reported literature data for the in-plane complex refractive index. The thickness dependence of peak size and location is thoroughly investigated by Yu et al. [16] and Song et al. [17] and attributed to decreasing excitonic binding, increasing joint density of states, and increasing mass density with the relative increase in film thickness. Unlike the previous published reports, the birefringence effect and corresponding out-of-plane optical properties of thin-film MoS₂ are also reported here. A recent pre-print also indicates the presence of anisotropy in the optical properties of exfoliated MoS₂.^[35] Our newly reported optical property data should be particularly useful in designing novel MoS2-based photonic devices such as UV photodetectors^[36] with monolayer and few-layer MoS₂ and photovoltaics^[37] with thin-film MoS₂.

For comparison, UV-Vis-NIR spectroscopy is used to measure the transmittance of the monolayer, few-layer, and thin-film MoS₂ samples. These samples were all grown on sapphire substrates, and transmittance through the bare substrate is used as a baseline correction. The measurements are done on relatively large areas of the samples (mm wide) with an integrating sphere, essentially giving a good average that accounts for spatial inhomogeneity. Figure 6a shows the transmittance versus wavelength for the samples between 190 and 1700 nm, the same spectral range for which the spectroscopic ellipsometry measurements are done. For the monolayer MoS2 sample, the excitonic A-C troughs are evident at around 670, 620, and 425 nm, respectively. [11,38] The few-layer sample also shows a trough at around 425 nm, whereas it is blue shifted for the thin-film sample. The thin-film sample shows two small troughs at around 670 and 620 nm as well. [11] For the monolayer and few-layer films, we see an additional trough in the UV at around 300 nm that is also consistent with our measured n and k values and previously published results. [20,21] The trough locations are consistent with the complex refractive index peak locations, between Figure 5 and 6a; the peaks from the complex refractive index plots correspond to troughs of the transmittance plots, because the complex refractive index is calculated from the reflection of polarized light.

4DVANCED

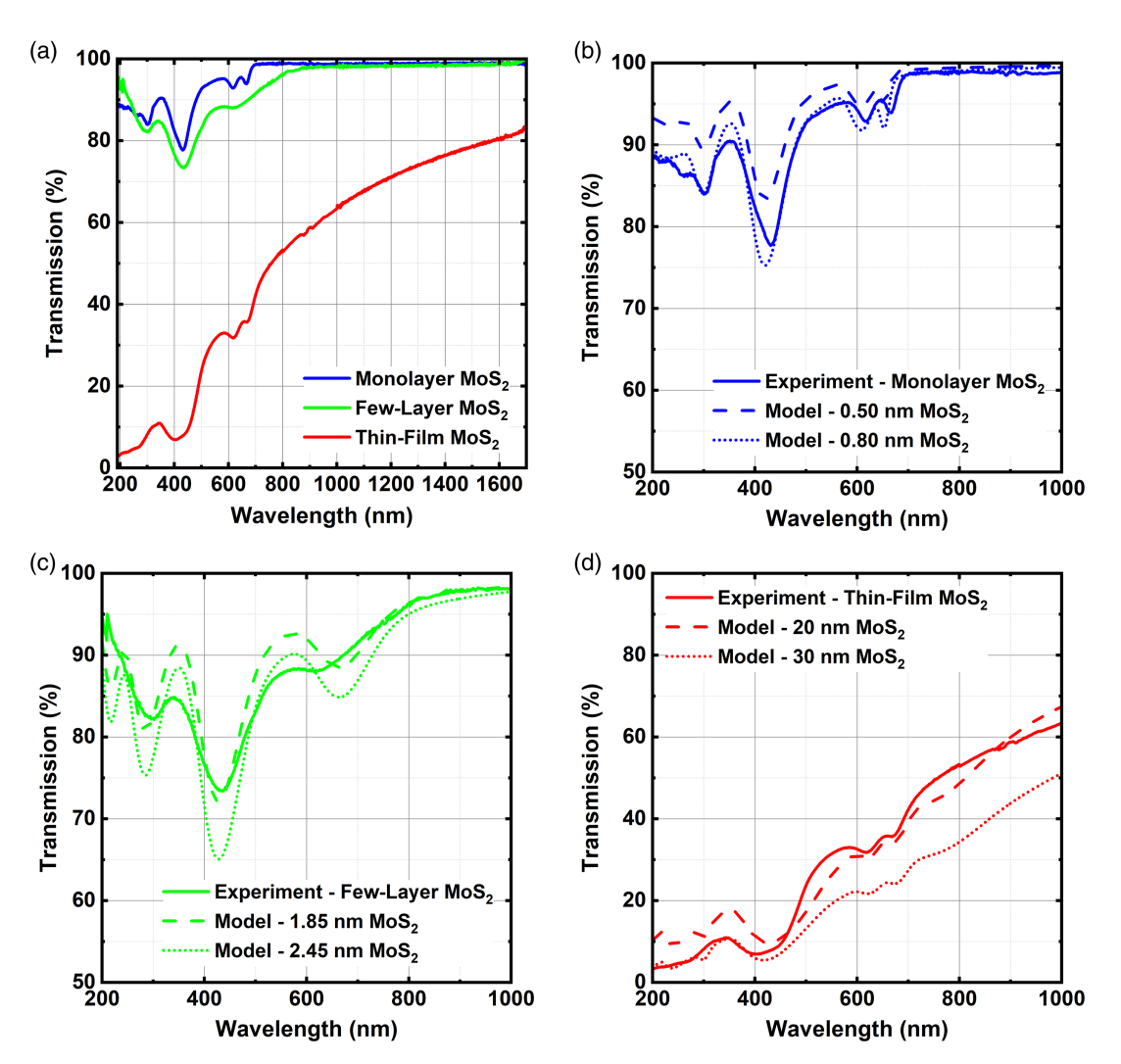


Figure 6. a) Measured transmittance of monolayer, few-layer, and thin-film MoS_2 samples grown directly on sapphire. Modeled transmittance of b) monolayer, c) few-layer, and d) thin-film MoS_2 samples overlaid with experimentally measured transmittance. The models use the complex refractive index data measured by spectroscopic ellipsometry, as shown in Figure 5 for specific film thicknesses.

To compare the data from the two fundamentally different measurements, a model is built to calculate transmittance through the bare monolayer, few-layer, and thin-film MoS_2 using the complex refractive index extracted from spectroscopic ellipsometry measurements and matched with the experimentally measured transmittance data. A good match between the two data sets assures confidence in the measurements and the derived material optical property data.

4. Optical Modeling

The model uses the TMM to calculate the transmittance, reflectance, and absorption in the MoS_2 active layer. [39,40] Figure 6b–d shows the modeled transmittance for different thicknesses of the stand-alone monolayer, few-layer, and thin-film MoS_2 overlaid with the measured transmittance of the same films. These figures are plotted between 200 and 1000 nm to highlight the

troughs and peaks clearly. In each calculation, the n and k data of the corresponding MoS_2 are used; i.e., for Figure 6b, the n and k data from monolayer MoS₂ are used, and so on. As shown in Figure 6b, the measured transmittance of the monolayer sample lies in between the calculated transmittance for 0.50 and 0.80 nm of MoS₂, confirming the monolayer thickness and validity of the complex refractive index data. The locations of the troughs for the modeled plots are slightly blue shifted compared with the experimental plot for the monolayer sample. This is because while experimental transmittance is measured for as-grown MoS2 samples on sapphire, the n and k data used in the models come from VASE measurements of transferred MoS₂ samples on SiO₂-on-Si substrates. As shown in Figure S7, Supporting Information, the excitonic peaks blue shift when transferred from sapphire to SiO₂-on-Si. In Figure 6c, the models are calculated for 1.85 and 2.45 nm, and the thickness for three layers and four layers of MoS₂, respectively. The transmittance matches better with the 1.85 nm MoS₂ sample, implying that the few-layer sample is

www advancedsciencenews com

www.adpr-journal.com

trilayer for the most part. For the thin-film MoS_2 sample, the transmittance matches closely with 30 nm of MoS_2 for the short wavelengths, whereas it has a better fit with 20 nm of MoS_2 in the longer wavelengths.

More details of the TMM are given in Section S6, Supporting Information. Given the complex nature of the refractive index of each material in the layer, the amount of light absorbed in the active layer can be determined as well from the TMM. [41,42] The absorption coefficient can be expressed in terms of the imaginary part of the refractive index known as the extinction coefficient, k, and the free space wavelength, λ . The amount of light absorbed in each layer can be estimated using the optical density or transmittance through the film using Lambert's law

$$\alpha = \frac{4\pi k}{\lambda}; \qquad I(x) = I_0 e^{-\alpha x} \tag{1}$$

where I(x) is the transmitted intensity after the light has been absorbed in the lossy medium, x is the thickness of the lossy medium, I_0 is the incident intensity of light, and α is the absorption coefficient.

Figure 7a shows the calculated absorption (%) for monolayer, few-layer, and thin-film MoS2 samples. The thickness used here for each sample is that from the AFM measurements, 0.61, 2.15, and 33.5 nm, respectively. The modeled results show that the monolayer, few-layer, and thin-film MoS₂ absorbs 7.4%, 12.6%, and 32.4% of the incident light, respectively, between 300 and 700 nm; again, they absorb 5.1%, 9.2%, and 26.1%, respectively, between 200 and 1000 nm. When normalized to per unitthickness absorption, between 300 and 700 nm, the monolayer MoS₂ absorbs 12.1% nm⁻¹; in comparison, the few-layer and thin-film MoS₂ absorbs 5.9% and 1.1% nm⁻¹, respectively, clearly showing superior light-matter interaction in the monolayer and few-layer films. Figure 7b shows the absorption (%) per unit-thickness (nm) versus wavelength for monolayer, fewlayer, and thin-film MoS₂. The plots are cropped between 200 and 800 nm to highlight the prominent excitonic absorption peaks in 2D MoS₂, i.e., monolayer and few-layer MoS₂, compared with the flat and low absorption profile of the thin-film MoS₂ sample.

As an example of the usefulness of this optical property data, the absorption models are further expanded to design optical coatings on top of the MoS_2 layers to either limit absorption within a specific spectral bandwidth or enhance broadband absorption in the MoS_2 active layers. The former is useful for designing photodetectors and sensors, whereas the latter is useful for designing photovoltaic solar cells using these 2D materials. The enhanced absorption is achieved by manipulating light–matter interaction in a given stack; the intrinsic optical properties of the active layer are not altered in any way. This modeling again utilizes the TMM.

Figure 8a,b shows the contour plots of absorption (%) in monolayer and few-layer MoS₂, respectively, between 200 and 800 nm for a range of TiO₂ thicknesses. The thickness of the monolayer and few-layer MoS₂ is set at 0.61 and 2.15 nm, respectively. While the monolayer and few-layer MoS₂ absorbs significantly in the UV as-is, a thin coating of TiO₂ on top can limit the absorption to the visible spectrum only. For example, the monolayer MoS₂ absorbs 7.8% of 200 nm monochromatic incident light, whereas with a 75 nm TiO₂ coating on top, the same absorption goes below 0.1%. The same is true for thin-film MoS₂; 100 nm of TiO₂ reduces few-layer MoS₂ absorption at 200 nm from 8.8% to \approx 0%. While complex structures are shown to be efficient in enhancing the absorption in monolayer MoS₂, [43] the same has not been achieved with a single-layer optical coating.

Figure 8c shows the broadband absorption versus wavelength in a thin-film MoS_2 layer for multiple thicknesses of indium tin oxide (ITO) as an anti-reflection coating (ARC). While different ITO thicknesses enhance the absorption in the MoS_2 layer in different parts of the spectrum, the maximum broadband absorption is achieved with 40 nm of ITO on top of the MoS_2 thin film, going from 29.1% without any ARC to 40.7%, for the 300–800 nm spectral range. In contrast, when the solar irradiance and spectrum are considered, 60 nm of ITO outperforms the other ITO thicknesses in terms of photocurrent generation in a photovoltaic device, as discussed in Section S7, Supporting Information.

Furthermore, various common ARCs are studied for enhanced broadband absorption in thin-film MoS₂, as shown in Figure 8d. A range of thicknesses for each ARC is considered,

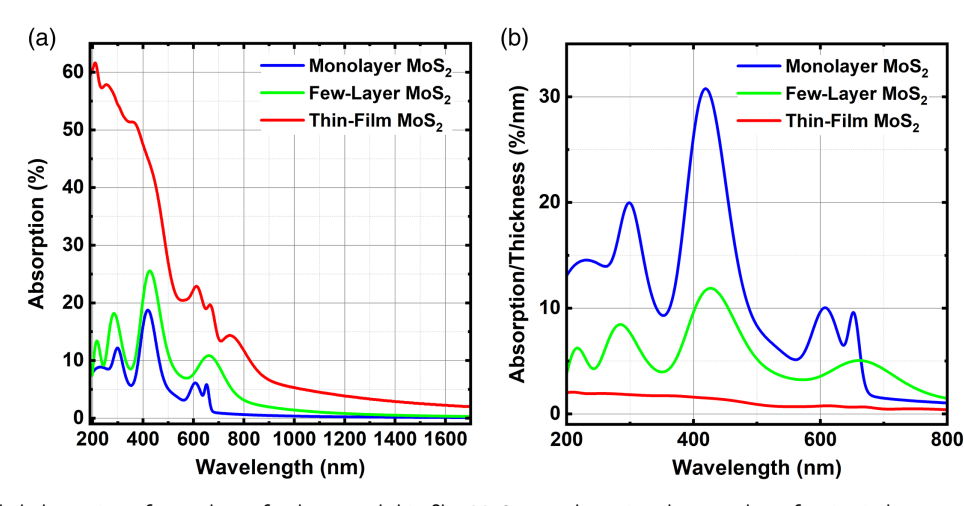


Figure 7. a) Modeled absorption of monolayer, few-layer, and thin-film MoS_2 samples using the complex refractive index measured by spectroscopic ellipsometry, as shown in Figure 4. b) Absorption per unit thickness is plotted versus wavelength.

www.advancedsciencenews.com www.adpr-journal.com

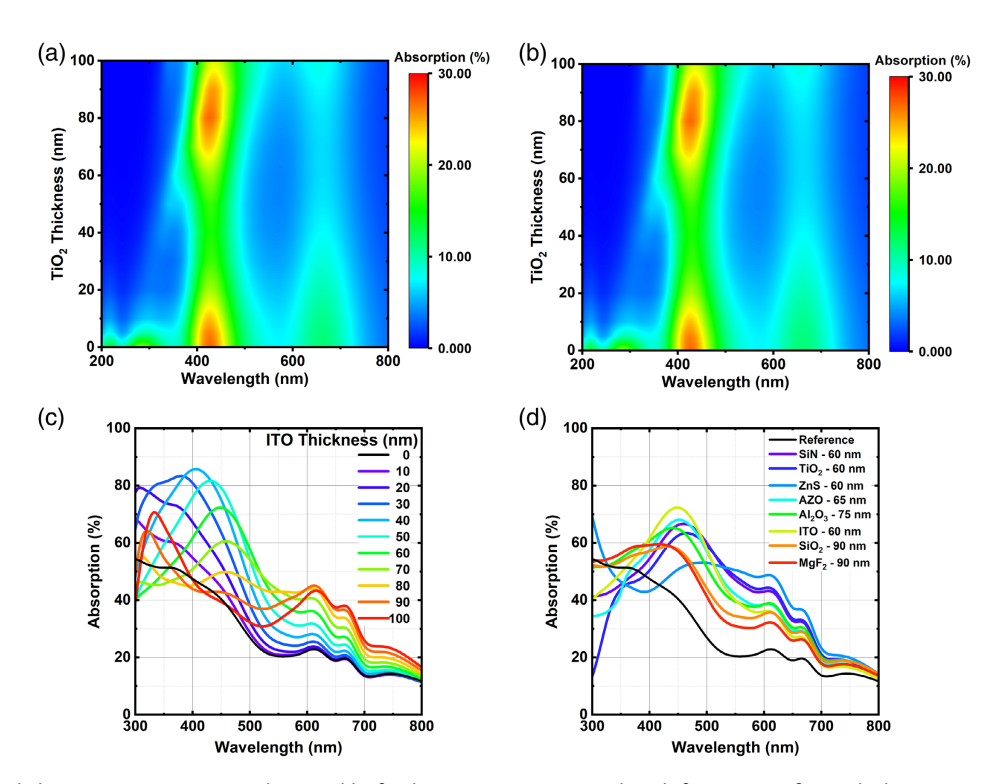


Figure 8. Calculated absorption (%) in a) monolayer and b) few-layer MoS_2 versus wavelength for a range of TiO_2 thickness on top. The optical stacks here are modeled as air— TiO_2 — MoS_2 —air, and only the absorption (%) in the active MoS_2 layers is plotted. c) Calculated absorption (%) in thin-film MoS_2 for a range of ITO thickness as an ARC. d) Various ARCs are studied to enhance the broadband absorption in thin-film MoS_2 .

and only the optimized thickness in terms of broadband absorption enhancement is shown in the figure. For example, 60 nm of SiN on top of the thin-film MoS_2 increases the broadband absorption between 300 and 800 nm by 44.1%, relatively, from 29.1% absorption without any ARC to 41.9% absorption with the addition of the SiN layer. The thickness of the thin-film MoS_2 layer is set to 35 nm for Figure 8c,d.

Finally, relatively thicker thin-film MoS₂ films are used in the model to maximize absorption for useful photovoltaic device application, and a maximum theoretical short-circuit current density (I_{sc}) is calculated assuming 100% internal quantum efficiency (IQE), as shown in Section S7, Supporting Information. The models show that 100 nm of the thin-film MoS₂ by itself absorbs 55.3% of the incident light between 300 and 800 nm, whereas an addition of 60 nm of ITO on top increases that absorption to 68.8%, a relative increase of 24.4%. On the other hand, 250 nm of the thin-film MoS₂ absorbs 77.9% and 59.4% with and without 60 nm of ITO on top in the same spectral range, respectively, showing a 31.1% relative increase. Finally, the $J_{\rm sc}$ of a photovoltaic device made with the 250 nm thin-film MoS₂ as an absorber layer can be enhanced from 20.3 to 26.8 mA cm⁻² with the addition of the 60 nm ITO coating, a 32% relative increase, assuming 100% IQE.

5. Conclusion

In summary, the monolayer, few-layer, and thin-film MoS₂ has been synthesized using the CVD and TVS methods. The complex

refractive indexes n and k of these samples have been extracted from VASE measurements for a broad spectral range between 190 and 1700 nm. The ellipsometry data showed sensitivity to optical birefringence in the thickest thin-film sample, and an analysis method was presented. The complex refractive index is then used to calculate reflectance, transmittance, and absorption of the MoS_2 films using TMM and matched with experimentally measured transmittance of the same samples.

One important way this study contributes to the broad scientific literature is by making the complex refractive index of 2D MoS₂ available for a large spectral range spanning the UV–Vis–NIR regions of the spectrum. This study also further guides how to design optoelectronic devices using simple optical coatings in conjunction with these 2D materials. Research is fast moving toward the realization of wearable, flexible, and transparent optoelectronic devices using 2D materials. Materials such as ITO may be used as a transparent conductive oxide, serving as ARCs to improve the broadband absorption of atomically thin photovoltaics made with 2D MoS₂ while eliminating the need for an opaque metal contact. To that end, the optical properties and results shown here are promising and significant for designing next-generation optoelectronic devices with 2D materials.

6. Experimental Section

Film Synthesis: The films are synthesized using an MTI OTF-1200X-II Dual Zone Split Tube Furnace that is modified to add a low-temperature third zone with a Grainger SRL series silicone heating blanket. The ACS reagent, $\geq 99.5\%$ molybdenum (VI) oxide (MoO₃), and the 99.98% trace

www advancedsciencenews com

www.adpr-journal.com

ADVANCED

metals basis sulfur (S) powder were bought from Sigma-Aldrich, whereas the molybdenum (Mo) pellets for electron-beam evaporation were purchased from Kurt J. Lesker Company.

Film Transfer. A surface-energy-assisted film transfer process developed by Gurarslan et al. $^{[26]}$ was used to transfer the MoS $_2$ films unto SiO $_2$ -on-Si substrate. Three to five drops of 15 wt% solution of polystyrene (PS) in toluene are spin-coated on to the as-grown MoS $_2$ film on sapphire at 500 rpm for 15 s and subsequently at 3250 rpm for 45 s; then, the PS-coated MoS $_2$ on sapphire is baked for 30 min at 90 °C. A water droplet is dropped on the sample followed by assisted penetration of the water between the PS/MoS $_2$ film and the sapphire substrate. Liftoff of PS/MoS $_2$ from the substrate is achieved by a slight needle insertion at the edge of the PS/MoS $_2$. The PS/MoS $_2$ is then transferred onto the SiO $_2$ -on-Si substrate and baked at 90 °C for 30 min to remove H $_2$ O, and then for 1 h at 130 °C to smooth out the transferred film. The PS is then rinsed off with toluene followed by a 24 h soak in toluene for complete removal of any PS residue.

Characterization Techniques: The PL characterization was done at 405 nm excitation wavelength using a Fianium (now NKT Photonics) super-continuum laser and Photon etc. laser line tunable filters. The laser spot size was $\approx 3~\mu m$ with 1 mW power. An Ocean Optics QEPro spectrometer is used for collecting PL signals with 1000 ms integration time and three-sample averaging. Raman characterization was conducted using a Thermo Scientific DXR Raman Microscope at 532 nm laser excitation wavelength with 5.0 mW laser power, 50 μm aperture slit, and a laser spot size of $\approx 2~\mu m$, with an estimated resolution of 5.5–8.3 cm $^{-1}$ between 3500 and 67 cm $^{-1}$ range. AFM measurements were performed using a Bruker Dimension FastScan system in ScanAsyst mode at 2 Hz frequency.

VASE data acquisition was performed using a J.A. Woollam RC2 spectroscopic ellipsometer running CompleteEASE software over the spectral range from 190 to 1700 nm. Data were acquired at five angles of incidence from 55° to 75° in steps of 5°. Ellipsometric Ψ and Δ data were acquired every 1 nm from 190 to 1000 nm, and every 2.5 nm from 1002.5 to 1700 nm.

Transmittance measurements were taken using a PerkinElmer LAMBDA 750S UV/Vis/NIR Spectrophotometer with a 60 mm integrating sphere between 190 and 1700 nm at 1 nm data interval and 1 s cycles. The photomultiplier tube (PMT) UV–Vis detector slit was fixed at 2 nm, whereas the InGaAs NIR detector slit was set to servo mode. The gains for the PMT and the InGaAs detector were set to auto and 1, respectively, while both detectors had a 0.20 s response time.

All characterization was done in air and at room temperature.

Supporting Information

Supporting Information is available from the Wiley Online Library or from the author.

Acknowledgements

This work was supported in part by the Carol Lavin Bernick Faculty Grant Program at Tulane University. The authors would like to acknowledge J. Wiley of the Advanced Materials Research Institute at the University of New Orleans for providing them access to their Raman spectroscopy tool. The authors would also like to acknowledge J. N. L. Albert, N. S. Pesika, and D. F. Shantz of the Chemical and Biomolecular Engineering Department at Tulane University for the use of their Bruker Dimension FastScan atomic force microscope.

Conflict of Interest

The authors declare no conflict of interest.

Data Availability Statement

The data that supports the findings of this study are available in the Supporting Information.

Keywords

2D materials, complex refractive index, molybdenum disulfide, spectroscopic ellipsometry, transition metal dichalcogenides

Received: December 10, 2020 Revised: January 19, 2021 Published online: March 9, 2021

- K. S. Novoselov, A. K. Geim, S. V. Morozov, D. Jiang, Y. Zhang, S. V. Dubonos, I. V. Grigorieva, A. A. Firsov, *Science* 2004, 306, 666.
- [2] M. Chhowalla, H. S. Shin, G. Eda, L. J. Li, K. P. Loh, H. Zhang, Nat. Chem. 2013, 5, 263.
- [3] E. Singh, P. Singh, K. S. Kim, G. Y. Yeom, H. S. Nalwa, ACS Appl. Mater. Interfaces 2019, 11, 11061.
- [4] A. Splendiani, L. Sun, Y. Zhang, T. Li, J. Kim, C. Y. Chim, G. Galli, F. Wang, Nano Lett. 2010, 10, 1271.
- [5] K. F. Mak, C. Lee, J. Hone, J. Shan, T. F. Heinz, Phys. Rev. Lett. 2010, 105, 136805.
- [6] B. Radisavljevic, A. Radenovic, J. Brivio, V. Giacometti, A. Kis, Nat. Nanotechnol. 2011, 6, 147.
- [7] G. Plechinger, J. Mann, E. Preciado, D. Barroso, A. Nguyen, J. Eroms, C. Schüller, L. Bartels, T. Korn, Semicond. Sci. Technol. 2014, 29, 064008
- [8] H. Li, Y. Li, A. Aljarb, Y. Shi, L. J. Li, Chem. Rev. 2018, 118, 6134.
- [9] S. Wang, Y. Rong, Y. Fan, M. Pacios, H. Bhaskaran, K. He, J. H. Warner, Chem. Mater. 2014, 26, 6371.
- [10] J. Robertson, X. Liu, C. Yue, M. Escarra, J. Wei, 2D Mater. 2017, 4, 045007.
- [11] Y. Li, A. Chernikov, X. Zhang, A. Rigosi, H. M. Hill, A. M. Van Der Zande, D. A. Chenet, E. M. Shih, J. Hone, T. F. Heinz, *Phys. Rev. B* 2014, 90, 1.
- [12] H. Li, Q. Zhang, C. C. R. Yap, B. K. Tay, T. H. T. Edwin, A. Olivier, D. Baillargeat, Adv. Funct. Mater. 2012, 22, 1385.
- [13] C. C. Shen, Y. Te Hsu, L. J. Li, H. L. Liu, Appl. Phys. Express 2013, 6, 8.
- [14] W. Li, A. G. Birdwell, M. Amani, R. A. Burke, X. Ling, Y. H. Lee, X. Liang, L. Peng, C. A. Richter, J. Kong, D. J. Gundlach, N. V. Nguyen, Phys. Rev. B 2014, 90, 1.
- [15] C. Hsu, R. Frisenda, R. Schmidt, A. Arora, S. M. de Vasconcellos, R. Bratschitsch, H. S. J. van der Zant, A. Castellanos-Gomez, Adv. Opt. Mater. 2019, 7, 1900239.
- [16] Y. Yu, Y. Yu, Y. Cai, W. Li, A. Gurarslan, H. Peelaers, D. E. Aspnes, C. G. Van De Walle, N. V. Nguyen, Y. W. Zhang, L. Cao, Sci. Rep. 2015, 5, 16996
- [17] B. Song, H. Gu, M. Fang, X. Chen, H. Jiang, R. Wang, T. Zhai, Y. T. Ho, S. Liu, Adv. Opt. Mater. 2019, 7, 1801250.
- [18] H. L. Liu, C. C. Shen, S. H. Su, C. L. Hsu, M. Y. Li, L. J. Li, Appl. Phys. Lett. 2014, 105, 201905.
- [19] C. Yim, M. O'Brien, N. McEvoy, S. Winters, I. Mirza, J. G. Lunney, G. S. Duesberg, Appl. Phys. Lett. 2014, 104, 103114.
- [20] D. Li, X. Song, J. Xu, Z. Wang, R. Zhang, P. Zhou, H. Zhang, R. Huang, S. Wang, Y. Zheng, D. W. Zhang, L. Chen, *Appl. Surf. Sci.* 2017, 421, 884.
- [21] J. W. Park, H. S. So, S. Kim, S. H. Choi, H. Lee, J. Lee, C. Lee, Y. Kim, J. Appl. Phys. 2014, 116, 183509.
- [22] G. A. Ermolaev, Y. V. Stebunov, A. A. Vyshnevyy, D. E. Tatarkin, D. I. Yakubovsky, S. M. Novikov, D. G. Baranov, T. Shegai, A. Y. Nikitin, A. V. Arsenin, V. S. Volkov, npj 2D Mater. Appl. 2020, 4, 1.

www.advancedsciencenews.com

www.adpr-journal.com

ADVANCED

- [23] H. G. Tompkins, W. A. McGahan, Spectroscopic Ellipsometry and Reflectometry, John Wiley and Sons, Ltd., New York 1999.
- [24] H. G. Tompkins, E. A. Irene, Handbook of Ellipsometry, William Andrew Publishing, Norwich, NY and Heidelberg, Germany 2005.
- [25] H. Fujiwara, Spectroscopic Ellipsometry: Principles and Applications, John Wiley & Sons, Tokyo 2007.
- [26] A. Gurarslan, Y. Yu, L. Su, Y. Yu, F. Suarez, S. Yao, Y. Zhu, M. Ozturk, Y. Zhang, L. Cao, ACS Nano 2014, 8, 11522.
- [27] W. H. Chae, J. D. Cain, E. D. Hanson, A. A. Murthy, V. P. Dravid, Appl. Phys. Lett. 2017, 111, 143106.
- [28] L. Wang, Z. N. Nilsson, M. Tahir, H. Chen, J. B. Sambur, ACS Appl. Mater. Interfaces 2020, 129, 15034.
- [29] C. M. Herzinger, B. Johs, W. A. McGahan, J. A. Woollam, W. Paulson, J. Appl. Phys. 1998, 83, 3323.
- [30] W. A. McGahan, B. Johs, J. A. Woollam, Thin Solid Films 1993, 234, 443.
- [31] B. D. Johs, W. A. McGahan, J. A. Woollam, Thin Solid Films 1994, 253, 25.
- [32] J. N. Hilfiker, N. Singh, T. Tiwald, D. Convey, S. M. Smith, J. H. Baker, H. G. Tompkins, *Thin Solid Films* 2008, 516, 7979.
- [33] H. Fujiwara, R. W. Collins, Spectroscopic Ellipsometry for Photovoltaics Volume 2: Fundamental Principles and Solar Cell Characterization, Springer, Berlin/New York **2018**.

- [34] N. Hong, R. A. Synowicki, J. N. Hilfiker, Appl. Surf. Sci. 2017, 421, 518.
- [35] G. A. Ermolaev, D. V. Grudinin, Y. V. Stebunov, V. G. Kravets, J. Duan, G. I. Tselikov, K. V. Voronin, D. I. Yakubovsky, S. M. Novikov, D. G. Baranov, A. Y. Nikitin, T. Shegai, P. Alonso-González, A. N. Grigorenko, A. V. Arsenin, K. S. Novoselov, V. S. Volkov, arXiv preprint 2020, arXiv:2006.00884.
- [36] G. Li, M. Suja, M. Chen, E. Bekyarova, R. C. Haddon, J. Liu, M. E. Itkis, ACS Appl. Mater. Interfaces 2017, 9, 37094.
- [37] A. J. Cho, M. K. Song, D. W. Kang, J. Y. Kwon, ACS Appl. Mater. Interfaces 2018, 10, 35972.
- [38] G. Eda, H. Yamaguchi, D. Voiry, T. Fujita, M. Chen, M. Chhowalla, Nano Lett. 2011, 11, 5111.
- [39] M. C. Troparevsky, A. S. Sabau, A. R. Lupini, Z. Zhang, Opt. Express 2010, 18, 24715.
- [40] C. C. Katsidis, D. I. Siapkas, Appl. Opt. 2002, 41, 3978.
- [41] G. F. Burkhard, E. T. Hoke, M. D. McGehee, Adv. Mater. 2010, 22, 3293.
- [42] L. A. A. Pettersson, L. S. Roman, O. Inganäs, J. Appl. Phys. 1999, 86, 487.
- [43] H. Lu, X. Gan, D. Mao, Y. Fan, D. Yang, J. Zhao, Opt. Express 2017, 25, 21630.